



ARTICLE

Small molecule QF84139 ameliorates cardiac hypertrophy via activating the AMPK signaling pathway

Xu-xia Li¹, Peng Zhang¹, Yang Yang², Jing-jing Wang³, Yan-jun Zheng¹, Ji-liang Tan¹, Shen-yan Liu^{1,3}, Yong-ming Yan², You-yi Zhang³, Yong-xian Cheng^{2,4} and Huang-tian Yang^{1,5,6}

Cardiac hypertrophy is a common adaptive response to a variety of stimuli, but prolonged hypertrophy leads to heart failure. Hence, discovery of agents treating cardiac hypertrophy is urgently needed. In the present study, we investigated the effects of QF84139, a newly synthesized pyrazine derivative, on cardiac hypertrophy and the underlying mechanisms. In neonatal rat cardiomyocytes (NRCMs), pretreatment with QF84139 (1–10 μM) concentration-dependently inhibited phenylephrine-induced hypertrophic responses characterized by fetal genes reactivation, increased ANP protein level and enlarged cardiomyocytes. In adult male mice, administration of QF84139 (5–90 $\text{mg}\cdot\text{kg}^{-1}\cdot\text{d}^{-1}$, i.p., for 2 weeks) dose-dependently reversed transverse aortic constriction (TAC)-induced cardiac hypertrophy displayed by cardiomyocyte size, left ventricular mass, heart weights, and reactivation of fetal genes. We further revealed that QF84139 selectively activated the AMPK signaling pathway without affecting the phosphorylation of CaMKII δ , ERK1/2, AKT, PKC ϵ , and P38 kinases in phenylephrine-treated NRCMs and in the hearts of TAC-treated mice. In NRCMs, QF84139 did not show additive effects with metformin on the AMPK activation, whereas the anti-hypertrophic effect of QF84139 was abolished by an AMPK inhibitor Compound C or knockdown of AMPK α 2. In AMPK α 2-deficient mice, the anti-hypertrophic effect of QF84139 was also vanished. These results demonstrate that QF84139 attenuates the PE- and TAC-induced cardiac hypertrophy via activating the AMPK signaling. This structurally novel compound would be a promising lead compound for developing effective agents for the treatment of cardiac hypertrophy.

Keywords: cardiac hypertrophy; pyrazine derivative; QF84139; phenylephrine; transverse aortic constriction; AMPK signaling pathway

Acta Pharmacologica Sinica (2022) 43:588–601; <https://doi.org/10.1038/s41401-021-00678-5>

INTRODUCTION

Cardiac hypertrophy is a response to the increased hemodynamic workload that arises from various physiological stimuli and pathological insults [1, 2]. It is characterized by an enlargement of myocardium with increases in cardiac mass and cardiomyocyte size, protein synthesis, and reactivation of fetal genes [1, 3]. Although it initially appears to be adaptive, the long-term cardiac hypertrophy is associated with a significantly increased risk of heart failure and ultimately leads to high rates of mortality and morbidity [4, 5]. Although much progress has been made in understanding the molecular mechanisms underlying cardiac hypertrophy, small molecules specifically targeting these pathways need to be discovered, which would allow to determine whether selectively regulating certain signaling pathways could reverse pathological hypertrophy [1] and help to develop new molecules for the treatment of patients with cardiac hypertrophy.

Development of cardiac hypertrophy to maladaptive is regulated by various signaling pathways, such as the calcium/calmodulin-dependent protein kinase type II delta (CaMKII δ), mitogen-activated protein kinase (MAPK) cascade including P38 kinase and extracellular signal-regulated kinase 1/2 (ERK1/2), protein kinase B (PKB/AKT), and protein kinase C epsilon (PKC ϵ) [1, 6–8]. One of the most important changes that promote cardiac hypertrophy is cardiomyocyte growth. Since the energy status of cells can dictate cell growth, it is likely that adenosine 5'-monophosphate-activated protein kinase (AMPK), a key regulator of cellular energy homeostasis, is importantly involved in the regulation of cell growth and hypertrophy [9, 10]. AMPK is a serine-threonine kinase consisting of a catalytic subunit (α) and 2 regulatory subunits (β , γ). The α 2 isoform of AMPK (AMPK α 2) is abundantly expressed in cardiomyocytes [11]. It participates in a variety of cellular processes to protect against cardiac hypertrophy [1, 10]. In pressure overload-induced cardiac hypertrophy, AMPK is

¹CAS Key Laboratory of Tissue Microenvironment and Tumor, Laboratory of Molecular Cardiology, Shanghai Institute of Nutrition and Health, University of Chinese Academy of Sciences, CAS, Shanghai 200031, China; ²State Key Laboratory of Phytochemistry and Plant Resources in West China, Kunming Institute of Botany, CAS, Kunming 650201, China; ³Department of Cardiology and Institute of Vascular Medicine, Peking University Third Hospital; NHC Key Laboratory of Cardiovascular Molecular Biology and Regulatory Peptides; Key Laboratory of Molecular Cardiovascular Science, Ministry of Education, Beijing Key Laboratory of Cardiovascular Receptors Research, Beijing 100191, China; ⁴School of Pharmaceutical Sciences, Health Science Center, Shenzhen University, Shenzhen 518060, China; ⁵Department of Cardiology, Shanghai Jiao Tong University Affiliated Sixth People's Hospital, Shanghai 200233, China and ⁶Institute for Stem Cell and Regeneration, CAS, Beijing 100101, China

Correspondence: Yong-xian Cheng (yxcheng@szu.edu.cn) or Huang-tian Yang (htyang@sibs.ac.cn)

These authors contributed equally: Xu-xia Li, Peng Zhang, Yang Yang

Received: 19 November 2020 Accepted: 2 April 2021

Published online: 9 May 2021

activated to preserve energy homeostasis [1, 10]. In addition, it can suppress protein synthesis via the inhibition of eukaryotic elongation and factor-2 (eEF2) kinase/eEF2 axis and mammalian target of rapamycin (mTOR)/p70 ribosomal protein S6 kinase (p70 S6K) pathway that are activated during hypertrophy [1, 10, 12, 13]. AMPK α 2 was reported to protect mouse hearts against transverse aortic constriction (TAC)-induced ventricular hypertrophy and dysfunction, in part, by repressing mTOR signaling [14]. AMPK has also been reported to inhibit cardiac hypertrophy through regulation of microtubule densification, autophagy, transcriptional activity, endoplasmic reticulum (ER) stress, and microRNA expression [1, 10, 15–17]. Pharmacological activation of AMPK, either by direct or indirect activators, can attenuate cardiac hypertrophy [8, 12, 18, 19]. These findings indicate crucial roles of the AMPK signaling pathway in the intervention of cardiac hypertrophy and suggest that AMPK activators might act as novel therapeutic reagents for cardiac hypertrophy. Therefore, the discovery of new AMPK activators would be valuable for the drug development against cardiac hypertrophy.

Natural products play a pivotal role for drug discovery [20]. Over 66% of new drugs based on small molecules approved by the US Food and Drug Administration between 1981 and 2019 are natural products and their direct derivatives or inspired by natural products [20]. Although the number of natural products is limited, millions of natural product hybrids (NPHs) as combinations of parts of different natural products can be developed and served as new leads for drug discovery [21].

Bearing this emerging concept in mind, we have purposely synthesized several NPHs aiming to discover new lead compounds for the treatment of heart associated disorders, including cardiac hypertrophy. In this study, using phenylephrine (PE)-induced cardiomyocyte hypertrophic cell model, we identified QF84139 as a candidate against cardiac hypertrophy. Then, we used the in vitro PE- and in vivo TAC-induced cardiac hypertrophy models, combining with signaling pathways screening and manipulation, to investigate (i) the effect of QF84139 in cardiac hypertrophy; and (ii) the signaling pathways involved in the anti-hypertrophic effects of QF84139. Our results demonstrated that QF84139 can attenuate cardiac hypertrophy via selectively activating the AMPK signaling pathway without affecting the CaMKII δ , ERK1/2, AKT, PKC ϵ , and P38 signaling pathways. Thus, QF84139 may act as a new activator of the AMPK signaling pathway used in the study of AMPK activation-related disorders and may have potential application value in the development of drugs for the treatment of cardiac hypertrophy.

MATERIALS AND METHODS

Preparation of QF84139

The small molecule used in this study (Code: QF84139) is a new compound, which was synthesized by a natural product derivative **2** and (–)-borneol (**3**) via a concise linker (–CH₂CO–). The target compound QF84139 was accomplished by three-step reactions with a 1.65% yield. The detailed reaction processes were as follows:

First step: the synthesis of **2** (QYY000, 5-(furan-2-yl)pyrazin-2(1H)-one) (Supplementary Fig. S2a): To a solution of SeO₂ (2.2 g, 20.5 mmol) in 30 mL of dioxane was added 1-(furan-2-yl)ethanone (1.5 g, 13.6 mmol) dissolved in dioxane and then refluxed for 8 h according to Sato's procedures [22]. The reaction mixture was filtrated and concentrated under reduced pressure to afford a mixture containing 1.3 g of 2-(furan-2-yl)-2-oxoacetaldehyde without purification. To a solution of 2-(furan-2-yl)-2-oxoacetaldehyde (1.3 g, 10.6 mmol) in 15 mL of methanol was added 2-aminoacetamide chloride (973 mg, 8.9 mmol) dissolved in 20 mL of methanol/water (2:1; at –30 °C), and then the sodium hydroxide (885 mg, 22.1 mmol) in 5 mL of water was dropped slowly into the solution. The reaction was kept for 90 min until the

temperature was back to 10 °C. The pH value of the resulting reaction mixture was adjusted to 3 at –10 °C with diluted hydrochloric acid, then filtrated and washed by water, dried in air to afford a yellow solid as QYY000 (5-(furan-2-yl)pyrazin-2(1H)-one (430 mg, 19.5% yield over 3 steps). ESIMS *m/z* 161 [M – H][–]; ¹H NMR (CDCl₃, 600 MHz) δ : 8.27 (1H, d, *J* = 1.5 Hz, H-2), 7.62 (1H, d, *J* = 1.5 Hz, H-4), 7.43 (1H, d, *J* = 1.8 Hz, H-8), 6.79 (1H, d, *J* = 3.3 Hz, H-6), 6.50 (1H, dd, *J* = 3.4, 1.8 Hz, H-7); ¹³C NMR (CDCl₃, 150 MHz) δ : 157.0 (C-1), 150.5 (C-5), 148.7 (C-2), 142.5 (C-8), 129.1 (C-3), 120.4 (C-4), 112.1 (C-7), 107.0 (C-6). Its planar structure was further identified by spectroscopic methods including ¹H NMR (Supplementary Fig. S3a), ¹³C NMR (Supplementary Fig. S3b).

Second step: the synthesis of QF84139 (Supplementary Fig. S2b): To a solution of (–)-borneol (**3**) (5.0 g, 32.5 mmol) as (1*S*,2*R*,4*S*)-1,7,7-trimethylbicyclo[2.2.1]heptan-2-ol, 2-bromoacetic acid (**4**) (9.0 g, 64.9 mmol) and DCC (13.4 g, 64.9 mmol) in dichloromethane at room temperature was slowly added 4-(dimethylamino)-pyridine (1.9 g, 15.6 mmol) dissolved in dichloromethane, stirred for 1 h. The resulting reaction mixture was filtrated and concentrated to afford **5** (4.2 g, 0.36 mmol, 47%). ¹H NMR (400 MHz, CDCl₃) δ : 4.88 (ddd, *J* = 10.0, 3.5, 2.1 Hz), 3.78 (s, 2H), 2.36 – 2.23 (m, 1H), 1.89 (m, 1H), 1.76 – 1.59 (m, 2H), 1.32 – 1.12 (m, 2H), 0.95 (dd, *J* = 14.0, 3.6 Hz, 1H), 0.84 (s, 3H), 0.81 (s, 3H), 0.79 (s, 3H); ¹³C NMR (100 MHz, CDCl₃) δ 167.5, 82.0, 49.0, 47.9, 44.7, 36.4, 27.9, 26.9, 26.3, 19.6, 18.8, 13.4.

To a solution of **2** (4.0 g, 14.6 mmol, QYY000) and K₂CO₃ (2.6 g, 19 mmol) in acetone was added into a solution of **5** (1*S*,2*R*,4*S*)-1,7,7-trimethylbicyclo[2.2.1]heptan-2-yl 2-bromoacetate (1.6 g, 9.7 mmol) dissolved in acetone, stirred at room temperature for 5 h, then filtrated and concentrated the solution to afford a yellow solid, after recrystallization with ethyl acetate and petroleum ether afforded 630 mg (18%) yellow solid as **6** (QF84139). QF84139: [α] –33 (c 0.20, CHCl₃); UV λ_{max} (MeOH) (log ϵ): 287 (3.71), 233 (3.54) nm; IR (KBr) ν_{max} 3427, 2956, 2881, 1741, 1679, 1622, 1455, 1386, 1360, 1306, 1216, 1116, 1019, 995 cm^{–1}; ESIMS *m/z* [M – H][–] 355; HRESIMS, calcd for C₂₀H₂₃N₂O₄: [M – H][–] 355.1663; found: 355.1656; ¹H NMR (CDCl₃, 600 MHz) δ : 8.23 (1H, brs, H-2), 7.47 (1H, brs, H-4), 7.38 (1H, brs, H-8), 6.75 (1H, d, *J* = 3.2 Hz, H-6), 6.47 (1H, dd, *J* = 3.2, 1.7 Hz, H-7), 4.98 (1H, ddd, *J* = 9.9, 3.1, 2.2 Hz, H-1'), 4.67 (2H, s, H-9), 2.35 (1H, m, H-6'a), 1.75 (1H, overlap, H-3'a), 1.75 (1H, overlap, H-4'a), 1.68 (1H, m, H-5'), 1.28 (1H, m, H-3'b), 1.20 (1H, m, H-4'b), 1.03 (1H, dd, *J* = 13.9, 3.3 Hz, H-6'b), 0.87 (3H, s, H-9'), 0.85 (3H, s, H-10'), 0.82 (3H, s, H-8'); ¹³C NMR (CDCl₃, 150 MHz) δ : 166.6 (C-1), 155.0 (C-1), 150.3 (C-5), 149.1 (C-2), 142.2 (C-8), 127.4 (C-3), 123.5 (C-4), 112.1 (C-7), 106.8 (C-6), 82.6 (C-1'), 50.5 (C-9), 49.1 (C-7'), 48.0 (C-2'), 44.8 (C-5'), 36.6 (C-6'), 28.0 (C-4'), 27.0 (C-3'), 19.7 (C-10'), 18.9 (C-9'), 13.6 (C-8').

Isolation of primary neonatal rat cardiomyocytes (NRCMs)

NRCMs were isolated as previously described [23, 24]. Briefly, the hearts were removed from 1-day-old Sprague Dawley (SD) rats, the atria was trimmed off, and then the tissue was minced by sequential digestion with 1 mg/mL collagenase II (Worthington, Lakewood, NJ, USA) and 0.125% trypsin. By differential plating, the ventricular cardiomyocytes were separated from fibroblasts and then cultured in gelatin-coated tissue culture plates in media containing Dulbecco's modified Eagle's medium (DMEM, Thermo Fisher Scientific, Waltham, MA, USA), 10% fetal bovine serum (Thermo Fisher Scientific, Waltham, MA, USA), 100 μ M bromodeoxyuridine (Sigma, Carlsbad, CA, USA), 1% penicillin-streptomycin (Thermo Fisher Scientific, Waltham, MA, USA), and 1% L-glutamine (Thermo Fisher Scientific, Waltham, MA, USA) with 95% air and 5% CO₂ at 37 °C for 24 h.

Cardiomyocyte hypertrophic cell model and screening of NPHs

The isolated NRCMs were cultured in the serum-free DMEM (Thermo Fisher Scientific, Waltham, MA, USA) for 12 h. Then the cells were treated with 10 μ M NPHs, 50 μ M resveratrol (RSV), or

vehicle and 1 h later were stimulated by 10 μ M PE (Sigma, Carlsbad, CA, USA) for 48 h in the presence of NPHs, RSV, or vehicle. The same protocol was used for the QF84139 treatment with various concentrations.

Cell viability assay

The Cell Counting Kit-8 (CCK-8, Sigma, Carlsbad, CA, USA) was used to determine cell viability as previously reported [24]. Briefly, the NRCMs were plated into 96 well plates for 24 h, and incubated with the medium containing indicated dosages of QF84139 or vehicle for 48 h. After treatment, the CCK-8 containing medium was added into each well for 4 h. The values were detected and analyzed by Synergy platereader (BioTek, Winooski, VT, USA).

Animals

Animals were cared complied with the Guidelines for Care and Use of Laboratory Animals published by the US National Institutes of Health (NIH Publication, 8th Edition, 2011). Experimental procedures involving animals were approved by the Institutional Animal Care and Use Committee of Shanghai Institutes for Biological Sciences (recently, it was named to Shanghai Institute of Nutrition and Health, Shanghai, China). Adult male C57BL/6 mice (10 weeks old) and neonatal SD rats (1 days) were purchased from Shanghai Slac Laboratory Animal Co. Ltd. AMPK α 2^{-/-} male mice (10 weeks) were kindly provided by Dr. Benoit Viollet (Institute National de la Santé et de la Recherche Médicale U567, Paris, France). The animals were allowed free access to food and water and were maintained on a 12 h light/dark cycle in a controlled temperature (20–22 °C) and humidity (50% \pm 5%) environment.

Mice TAC surgical procedure and study design

The mice TAC model was used to induce cardiac hypertrophy as described previously [23]. Briefly, male mice (10 weeks) were anaesthetized with pentobarbital sodium (50 mg/kg) by intraperitoneal (i.p.) injection and placed on a temperature (37 °C)-controlled surgical table. Volume-regulated respirator (SAR830, Cwe Incorporated, Ardmore, PA, USA) at a frequency of 90 bpm and the tidal volume ranged 200–300 mL/min was used to ventilate. The mice were divided into Sham and TAC groups. A longitudinal cut was made in the proximal portion of the sternum. A 7-0 silk suture was placed around the aorta between the right innominate artery and left common carotid artery. The suture was tied around a 27-gauge needle and the aorta. After ligation in place, the needle was promptly removed. Sham-operated mice underwent the same procedure but without ligation around the aorta. At the same day after aortic constriction, TAC-operated wild-type (WT) mice were randomly divided into five groups: TAC + vehicle and four TAC + QF84139 groups with the administration of QF84139 at 5 mg·kg⁻¹·d⁻¹, 15 mg·kg⁻¹·d⁻¹, 45 mg·kg⁻¹·d⁻¹, and 90 mg·kg⁻¹·d⁻¹, respectively (i.p.). Sham-operated WT mice were randomly divided into two groups: Sham + vehicle and Sham + QF84139 (90 mg·kg⁻¹·d⁻¹, i.p.). The TAC-operated AMPK α 2^{-/-} mice were randomly divided into two groups: TAC + vehicle, TAC + QF84139 (15 mg·kg⁻¹·d⁻¹, i.p.). Sham-operated AMPK α 2^{-/-} mice were randomly divided into two groups: AMPK α 2^{-/-} Sham + vehicle and AMPK α 2^{-/-} Sham + QF84139 (15 mg·kg⁻¹·d⁻¹, i.p.). The vehicle and QF84139 were administered once per day, from day 1 to day 14 post-surgery at the same volume. At the end of the study, animals were anaesthetized with an overdose of sodium pentobarbital (200 mg/kg, i.p.) as previously described [9], and the hearts, lungs, livers, spleens, kidneys, and tibia were collected.

Small interfering RNA for AMPK α 2 (si-AMPK α 2)

Oligonucleotide sequences were purchased from Ribobio to prepare small interfering RNA for AMPK α 2. The siRNA sequences were as follows: AMPK α 2 siRNA, 5'-CGTCATTGATGATGAGGCT-3',

and scrambled siRNA, 5'-AUUGUAUGCGAUCGCAGAC-3'. Scrambled siRNA was used as a control in all experiments. NRCMs were transfected with Scrambled siRNA (4 μ g) or AMPK α 2 siRNA (2 μ g) using DharmaFECT 1 transfection reagent (Thermo Fisher Scientific, Waltham, MA, USA) according to the manufacturer's instruction for 24 h and then with QF84139 for another 1 h prior to PE treatment.

Echocardiography

Cardiac function and structure were performed as previously described [24]. Briefly, the Vevo2100 imaging system (Visual Sonics, Toronto, Canada) with 30 MHz linear transducer probe (MS400D) was used for two-dimensional B-mode and M-mode analyses. The heart rate was maintained at 450–550 bpm via isoflurane anesthesia (1.5%–2%, 2 L/min oxygen flow rate). Normal body temperature was maintained. The mitral valve leaflet was visualized and cardiac function was assessed at long axis B-mode view by placing the transducer on the left lateral chest wall. Measurements were recorded as the mean of at least three consecutive cardiac cycles. Left ventricular (LV) internal dimension (LVID;s) in systole and left ventricular internal dimension diastole (LVID;d), thickness of the interventricular septum in systole (IVS;s) and interventricular septum in diastole (IVS;d) and thickness of the LV posterior wall in systole and diastole (LVPW;s and LVPW;d, respectively) were obtained from the echocardiograms. Using the following formula: EF (%) = [(LVvol;d - LVvol;s)/LVvol;d] \times 100, the LV ejection fraction (EF) was calculated; and the LV fractional shortening (FS) was calculated using FS (%) = [(LVID;d - LVID;s)/LVID;d] \times 100.

Histological analysis

Histological examination was performed as previously described [23, 25]. Briefly, the mice hearts from each group were quickly harvested, and washed with 5 mL cold cardiac arresting buffer (10% KCl), phosphate buffered saline (PBS), fixed with 4% paraformaldehyde for 48 h, and then embedded in paraffin. The LV cross sections at 5 μ m thick were deparaffinized by immersing in xylene, and rehydrated and then stained with hematoxylin-eosin (H&E) and FITC-labeled wheat germ agglutinin (WGA, Thermo Fisher Scientific, Waltham, MA, USA). All of the immunofluorescence images were blindly taken with a Zeiss microscope. The Image-processing software (ImageJ) was used to analyze the cross-sectional area of cardiomyocytes.

Immunofluorescence analysis

For immunofluorescence, cardiomyocytes grown in 6-well plates were washed three times with phosphate-buffered saline (PBS) after PE treatment for 48 h and fixed with 4% (w/v) paraformaldehyde for 30 min at room temperature. Then the cells were permeabilized in 0.3% Triton X-100, blocked in 10% normal goat serum (Vector Laboratories, Burlingame, CA, USA) and then incubated with primary antibodies α -actinin (1:200, Abcam, Cambridge, UK) and atrial natriuretic peptide (ANP) (1:200, Bioworld, Dublin, OH, USA) at 4 °C overnight before the secondary antibodies (1:500, Thermo Fisher Scientific, Waltham, MA, USA). Negative controls were performed with secondary antibody-only staining. Nuclei were stained with DAPI (Sigma-Aldrich, Carlsbad, CA, USA). Images were taken using a Zeiss Cell Observer confocal laser scanning microscope 710 (Zeiss, Germany) and processed using ZEN software. Fluorescence images were analyzed with ImageJ.

Quantitative reverse transcription polymerase chain reaction (qRT-PCR)

Total RNA was extracted from mouse LVs or NRCMs using Trizol (Invitrogen, Carlsbad, CA, USA) or RNeasy Mini kit (QIAGEN, Hilden, Germany) following the manufacturer's instruction and analyzed by qRT-PCR as previously described [24]. Briefly, cDNA was generated by reverse-transcribed total RNA (1 μ g) using oligo

(dT) primer and ReverTra Ace reverse transcriptase (TOYOBO, Japan). Taq DNA Polymerase (Takara, Japan) was used to carry out PCR. qRT-PCR was performed using an ABI VII7 system (Applied Biosystems, Foster City, CA, USA) with the SYBR Green Real-time PCR Master Mix plus (TOYOBO, Japan) for relative quantification of the indicated genes. The amplification program was performed as follows: 94 °C for 10 min and 30 cycles at 94 °C for 30 s, 55 °C for 30 s, and 72 °C for 30 s. The transcript of GAPDH was used for internal normalization. The sequences of primer pairs are listed in Supplementary Table S1.

Western blot analysis

Mice LV were homogenized and the proteins were extracted as previously described [26]. Briefly, about 50 mg of left ventricular tissues were homogenized on ice with a homogenizer in 10 vols of immunoprecipitation assay (RIPA) lysis buffer containing 1% Triton X-100, 5 mmol/L 2-mercaptoethanol, and 1% deoxycholate, 10% glycerin, 150 mM NaCl, 2.5 mM EDTA and 1 mg/mL protease inhibitor cocktail. For cultured cells, the NRCMs were scraped into RIPA lysis buffer containing protease inhibitor cocktail (Roche, Mannheim, Germany), 50 mM Tris-HCl (pH 7.4), 150 mM NaCl, 1% NP-40, 0.5% deoxycholate and 1 mM EDTA, followed by vigorous vortexing and cooling on ice for 15 min before centrifugation at 12,000 × *g* for 15 min. The concentration of proteins was determined by the bicinchoninic acid assay (BCA) using the Pierce BCA Protein Assay Kit (Thermo Fisher Scientific, Waltham, MA, USA). The homogenates/lysates were stored at −80 °C. Tissue homogenates and whole cell lysates were analyzed by standard immunoblotting. The proteins (20 µg) were loaded and detected by specific antibodies against ANP (1:2000, Bioworld, Dublin, OH, USA), GAPDH (1:8000, CST, Danvers, MA, USA), PKCε (1:1000, Millipore, Burlington, MA, USA), phospho-PKCε (1:1000, Abcam, Cambridge, UK), CaMKIIδ (1:1000, Abcam, Cambridge, UK), phospho-CaMKIIδ (1:1000, Sigma, Carlsbad, CA, USA), ERK (1:1000, CST, Danvers, MA, USA), phospho-ERK (1:1000, CST, Danvers, MA, USA), AKT (1:1000, CST, Danvers, MA, USA), phospho-AKT (1:1000, CST, Danvers, MA, USA), P38 (1:1000, CST, Danvers, MA, USA), phospho-P38 (1:1000, CST, Danvers, MA, USA), AMPK (1:1000, Abcam, ab3769), phospho-AMPK (T172, 1:1000, CST, Danvers, MA, USA), AMPKα2 (1:1000, CST, Danvers, MA, USA), ACC (1:1000, CST, Danvers, MA, USA), phospho-ACC (Ser79, 1:1000, CST, Danvers, MA, USA), mTOR (1:2,000, CST, Danvers, MA, USA), phospho-mTOR (Ser2448, 1:2000, CST, Danvers, MA, USA), p70 ribosomal protein S6 kinase (P70 S6K) (1:1000, CST, Danvers, MA, USA), phospho-P70 S6K (Thr389, 1:1000, CST, Danvers, MA, USA), eukaryotic translation initiation factor 4E-binding protein 1 (4E-BP1) (1:1000, CST, Danvers, MA, USA), and phospho-4E-BP1 (Thr37/46, 1:1000, CST, Danvers, MA, USA). The immunoreaction was visualized with an enhanced ECL detection kit (PerkinElmer Life, Waltham, MA, USA) and then exposed to film and quantified with Quantity One. The densitometry analysis of immunoblots was conducted in a double-blinded fashion.

Statistical analysis

Data were expressed as means ± SEM. Statistical analysis for comparison between two groups was performed using two-tailed unpaired *t* test. Statistical analysis for comparison in multiple groups was performed using one-way or two-way ANOVA followed by Dunnett's multiple comparisons post hoc test. Analyses were performed with GraphPad Prism v 8.0. *P* value < 0.05 was considered statistically significant.

RESULTS

Screening of anti-hypertrophic compounds from NPHs

We screened anti-hypertrophy compounds from a library of 24 compounds derived from insects and plants or synthesized derivatives using an in vitro PE-induced hypertrophic model in

NRCMs. Resveratrol (RSV) was used as positive control. After 10 µM of PE treatment for 48 h, the mRNA expression of *ANP*, a hypertrophy marker gene, was significantly increased (Supplementary Fig. S1), indicating a hypertrophic response in NRCMs. Among the 24 compounds examined, QF84139 and RSV significantly attenuated the expression of *ANP* induced by PE, suggesting the anti-hypertrophic effect of QF84139.

Preparation of QF84139 by total synthesis

QF84139 is a small-molecular compound totally synthesized via three steps starting respectively from 1-(furan-2-yl) ethanone and (−)-borneol (for details, see "Materials and methods"). The chemical structure is shown in Fig. 1a. Its planar structure was further identified by spectroscopic methods including ¹H NMR (Supplementary Fig. S4a), ¹³C NMR (Supplementary Fig. S4b), ¹H-¹H COSY (Supplementary Fig. S5a), HSQC (Supplementary Fig. S5b), HMBC (Supplementary Fig. S5c), ROESY (Supplementary Fig. S5d), and HRESIMS spectrum (Supplementary Fig. S6a). The absolute configuration of QF84139 was assigned as 1*S*, 2*R*, 4*S* because that (−)-borneol which possesses a known configuration was used as a building block. The purity of QF84139 was verified by HPLC analysis (Supplementary Fig. S6b and c).

QF84139 inhibits PE-induced hypertrophic responses in NRCMs

To evaluate the cytotoxicity of QF84139 in cardiomyocytes, a standard CCK-8 assay was performed. Compared with the control group, the cell viability did not differ after QF84139 treatments at the concentrations from 0.3 µM to 100 µM for 2 days (Supplementary Fig. S7). The anti-hypertrophic effect was firstly detected using the in vitro PE-induced NRCM hypertrophic model with various concentrations of QF84139 given 1 h before PE stimulation as shown in the schematic of the cell model and treatments (Fig. 1b). The mRNA expression level of *ANP*, brain natriuretic peptide (BNP), and β-myosin heavy chain (β-MHC) was significantly increased by 10 µM of PE treatment for 48 h. However, the PE-increased gene expression was inhibited by QF84139 in a concentration-dependent manner and was reversed to the basal level at 3 µM of QF84139 (Fig. 1c–e). We thus used 3 µM of QF84139 for the following experiments. The immunostaining analysis further validated that the PE-enhanced protein level of *ANP* was significantly inhibited by QF84139 (Fig. 1f). Moreover, the PE stimulation-increased cell size was reduced by QF84139 (Fig. 1g). QF84139 alone did not affect the protein level of *ANP* (Fig. 1f) and the cell size (Fig. 1g). These data demonstrate that QF84139 attenuates hypertrophic response in NRCMs.

QF84139 alleviates pressure overload-induced cardiac hypertrophy in WT mice

To further evaluate the effect of QF84139 on the process of cardiac hypertrophy, we used TAC-induced cardiac hypertrophy model in WT adult male C57BL/6 mice. The vehicle or QF84139 was administered right after the Sham or TAC operation via intraperitoneal injection at different doses daily for 2 weeks (Fig. 2a). The mice under vehicle and QF84139 treatments exhibited comparable appearance (Supplementary Fig. S8a), organ shape and color (Supplementary Fig. S8b), and organ weight (lung (Supplementary Fig. S10e, f), liver (Supplementary Fig. S8c, f), spleen (Supplementary Fig. S8d, g) and kidney (Supplementary Fig. S8e, h)). The body weight (Supplementary Fig. S9a) and heart rate (Supplementary Fig. S9b) were comparable between the mice with or without the QF84139 treatment either in Sham and TAC groups. The echocardiographic analysis showed that TAC-induced increases in LVPW;d, LVPW;s, LVS;d, LVS;s, and LV mass and decrease in LVID;d were significantly attenuated by QF84139 in a dose-dependent manner and these parameters were not affected by QF84139 in the Sham mice (Fig. 2b–h) even though the LVID;s, EF, and FS (Supplementary Fig. S10a–c) remained unchanged. Consistently, HE and WGA staining demonstrated that the

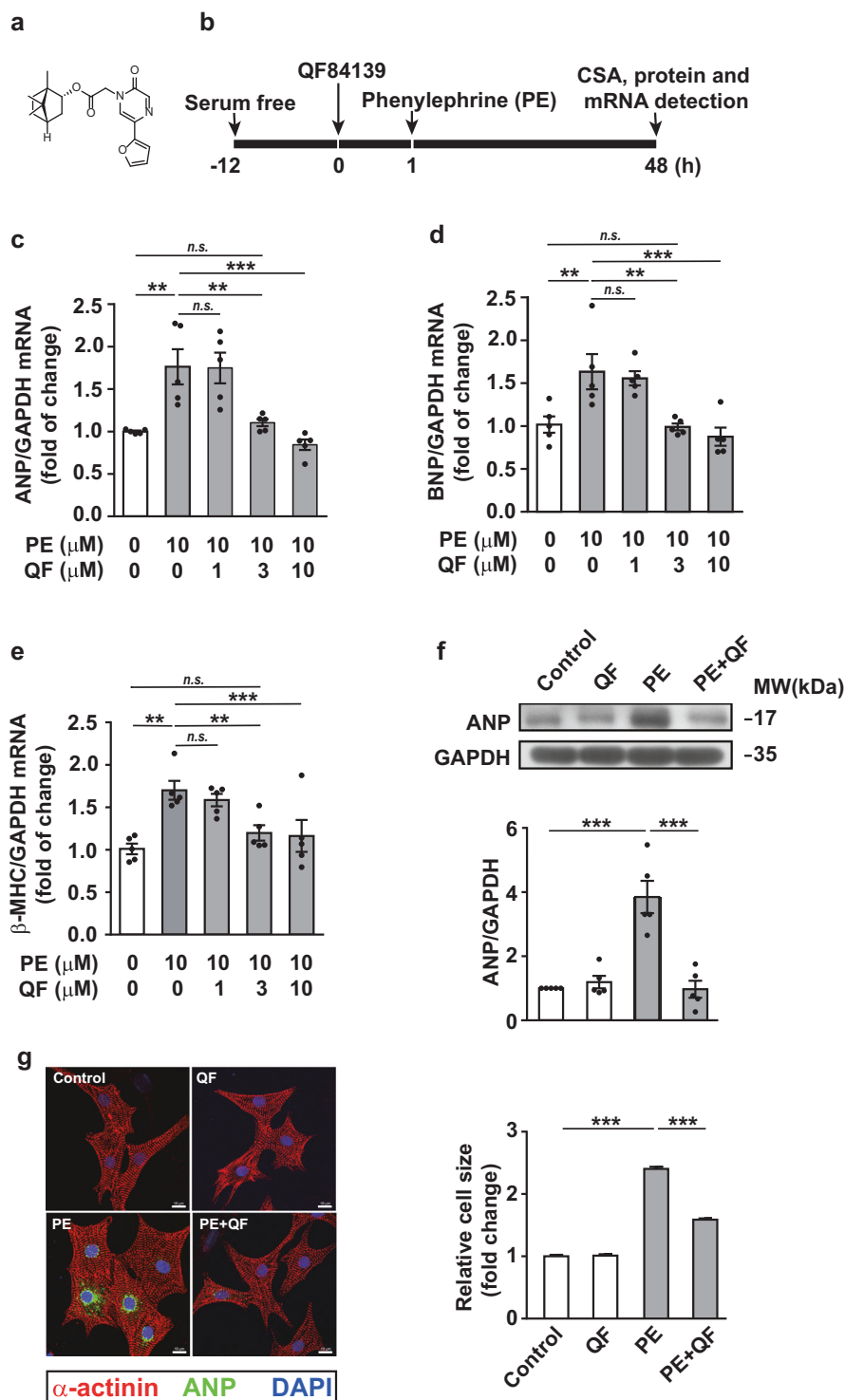


Fig. 1 QF84139 (QF) inhibits phenylephrine (PE)-induced cardiac hypertrophic responses in vitro. Neonatal cardiac myocytes (NRCMs) treated with various concentrations of QF or vehicle for 1 h before the cells were treated with PE (10 μM) for 48 h. **a** The chemical structure of QF84139. **b** Schematic of PE and QF treatment. qRT-PCR analysis of mRNA expression of ANP (**c**), BNP (**d**) and β-MHC (**e**). $n = 5$ each. **f** Immunoblot analysis of ANP protein with or without QF (3 μM) and PE (10 μM) treatments $n = 5$. **g** Representative images (left panels) and averaged cell size (right panels) for immunofluorescence staining with anti-α-actinin antibody (red), anti-ANP antibody (green), and DAPI (blue) in NRCMs treated with vehicle or QF (3 μM) in the absence or presence of PE (10 μM). Scale bar = 10 μm. $n = 200$ from 3 individual experiments. $**P < 0.01$, $***P < 0.001$. n.s., nonsignificant

enlargement of cardiomyocytes in TAC mice was significantly inhibited by the QF84139 treatment (Fig. 3a). The quantified cross-sectional area further confirmed the dose-dependent anti-hypertrophic effect of QF84139 (Fig. 3b). Moreover, the enhanced

expression of hypertrophic marker genes ANP, BNP, and β-MHC in hearts from TAC mice were suppressed by QF84139 treatment, whereas these parameters remained unchanged in the Sham-operated mice treated with QF84139 when compared with

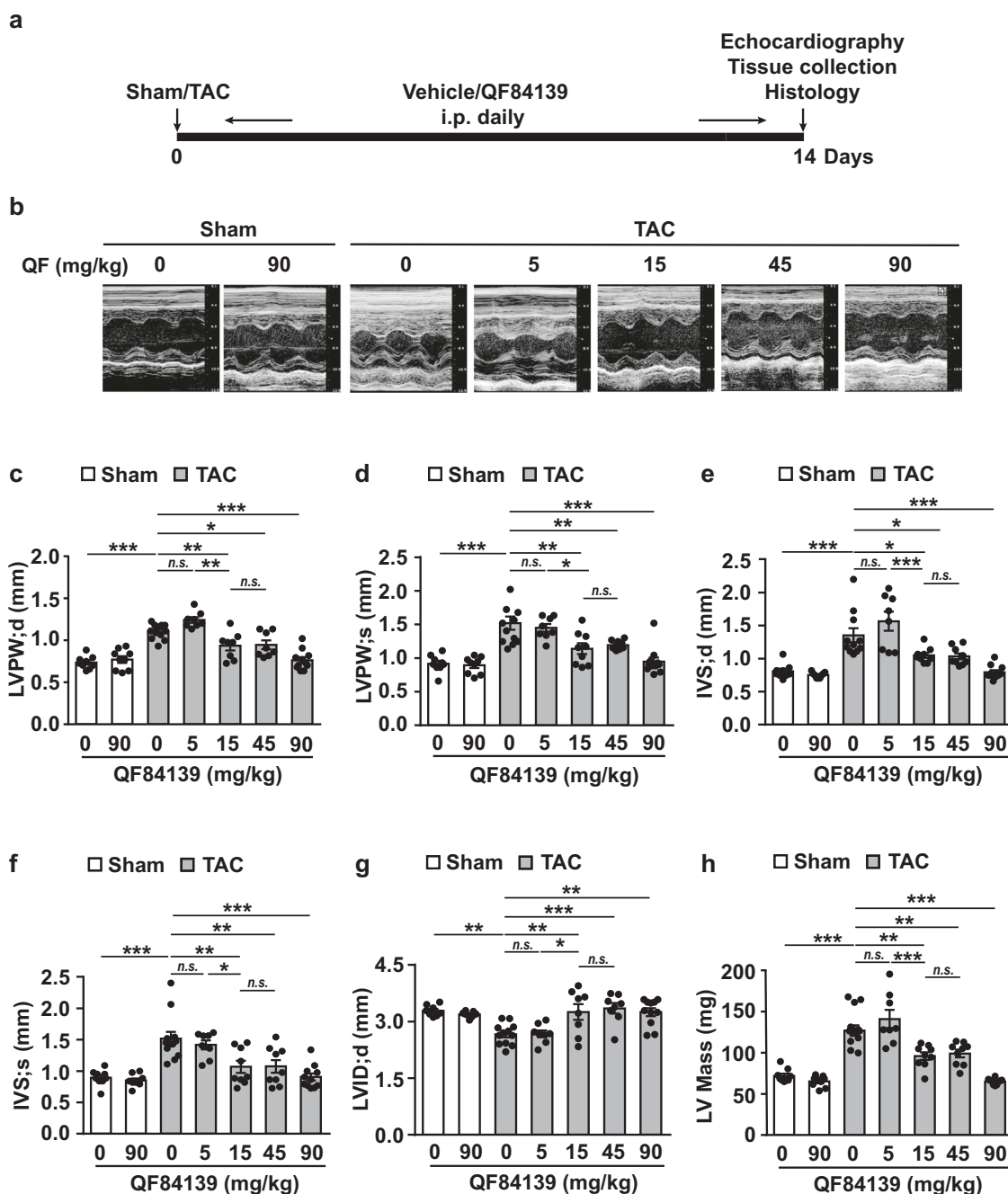


Fig. 2 QF84139 (QF) dose-dependently attenuates transverse aortic constriction (TAC)-induced cardiac dysfunction in wild-type (WT) mice at 2 weeks post-TAC or Sham surgery. **a** Schematic diagram of QF84139 treatment and analysis. **b** Representative images of echocardiograms. **c** LVPW;d, left ventricle posterior wall thickness diastole. **d** LVPW;s, left ventricle posterior wall thickness systole. **e** IVS;d, interventricular septum diastolic dimension. **f** IVS;s, interventricular septum systolic dimension. **g** LVID;d, left ventricular internal dimension in diastole. **h** LV Mass, left ventricle mass. $n = 8-11$ per group. * $P < 0.05$, ** $P < 0.01$, *** $P < 0.001$. n.s., nonsignificant

the vehicle group (Fig. 3c–e). Moreover, the TAC mice exhibited markedly increased ratios of heart weight/tibia length (HW/TL, Fig. 3f), heart weight/body weight (HW/BW, Supplementary Fig. S10d), lung weight/tibia length (LW/TL, Supplementary Fig. S10e), and lung weight/body weight (LW/BW, Supplementary Fig. S10f) compared with the Sham-operated group. However, these alterations were reversed by the administration of QF84139 in a dose-dependent manner and a significant inhibition was observed at $15 \text{ mg} \cdot \text{kg}^{-1} \cdot \text{d}^{-1}$ of QF84139 (Fig. 3f). Furthermore, the gross hearts and whole hearts with H&E staining confirmed that QF84139 treatment at $15 \text{ mg} \cdot \text{kg}^{-1} \cdot \text{d}^{-1}$ inhibited the larger

heart size induced by TAC (Fig. 3g). Taken together, these data demonstrate that QF84139 prevents the TAC-induced development of ventricular hypertrophy in the WT mice.

QF84139 activates AMPK in the hypertrophic NRCMs and mice hearts

To identify signaling pathways involved in the anti-hypertrophic effect of QF84139, we then screened protein kinases which may regulate cardiac hypertrophy reported previously [1, 6–8]. In NRCMs, the phosphorylation levels of CaMKII δ , ERK, AKT, PKC ϵ , and P38 were significantly increased after PE treatment, while

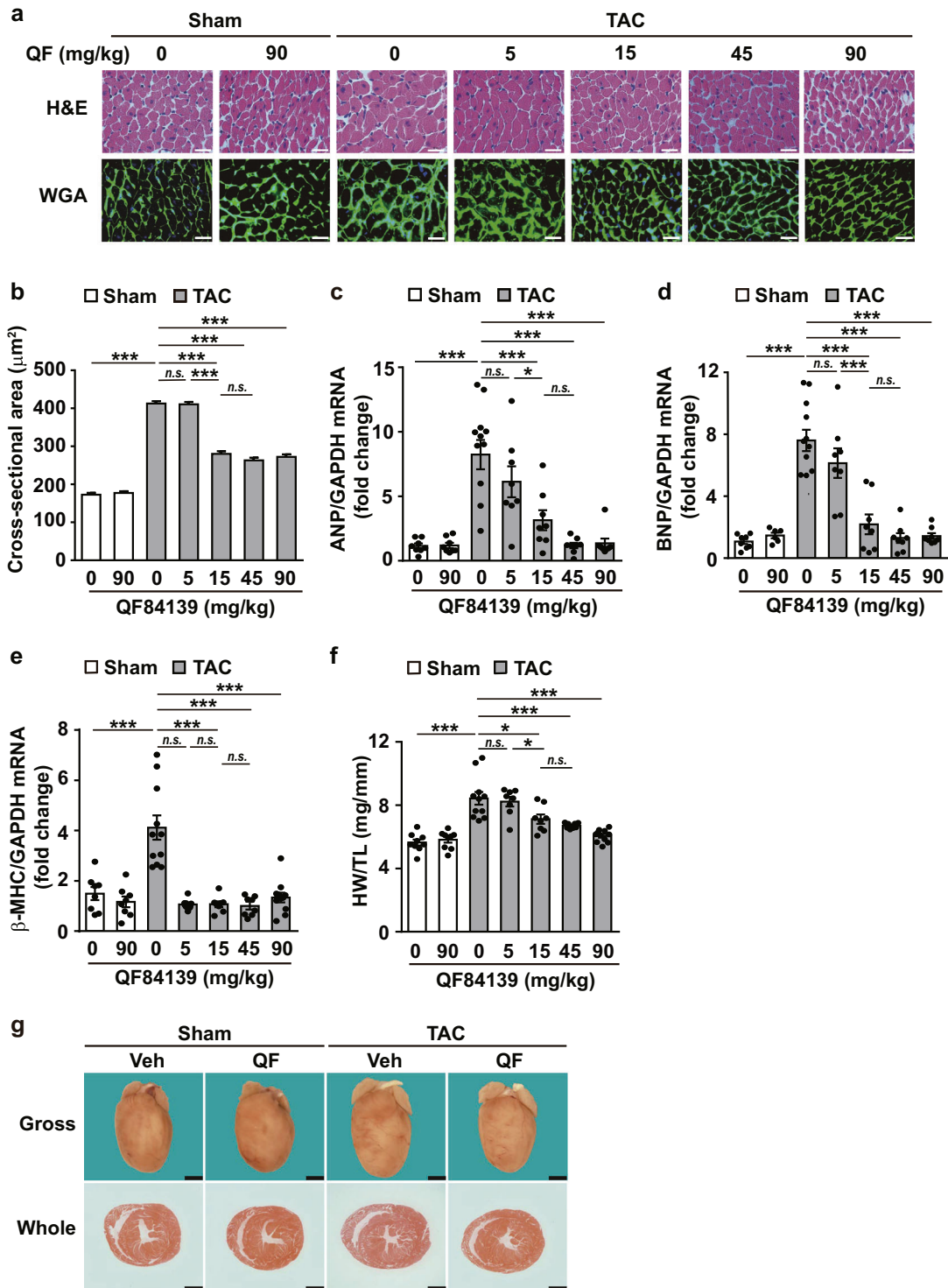


Fig. 3 QF84139 (QF) dose-dependently attenuates TAC-induced cardiac hypertrophy in WT mice at 2 weeks post-TAC or sham surgery. **a** H&E staining and WGA staining analysis of hypertrophic growth of cardiomyocytes. Scale bar = 20 µm. **b** Quantification of the size of cardiomyocytes by measurement of the cross-sectional area (200 random cells/heart, $n = 3$ hearts per groups). qRT-PCR analysis of mRNA expression levels of ANP (**c**), BNP (**d**), and β -MHC (**e**). $n = 8-11$. **f** Statistical results of heart weight/tibia length ratio (HW/TL). $n = 8-11$. **g** Representative gross hearts (top) and whole hearts sections stained by H&E (bottom) of adult hearts from WT mice with or without vehicle (Veh) or 15 mg·kg⁻¹·d⁻¹ of QF. Scale bars = 1 mm. * $P < 0.05$, *** $P < 0.001$. n.s., nonsignificant

their total protein levels remained unchanged compared with the control ones (Supplementary Fig. S11). Intriguingly, the PE-enhanced phosphorylation levels of these protein kinases were not significantly affected by QF84139 treatment (Supplementary

Fig. S11). Notably, the total protein and phosphorylation levels of AMPK remained unchanged in the PE-treated NRCMs, whereas the phosphorylation levels of AMPK were significantly increased after QF84139 treatment in both groups with or without PE stimulation

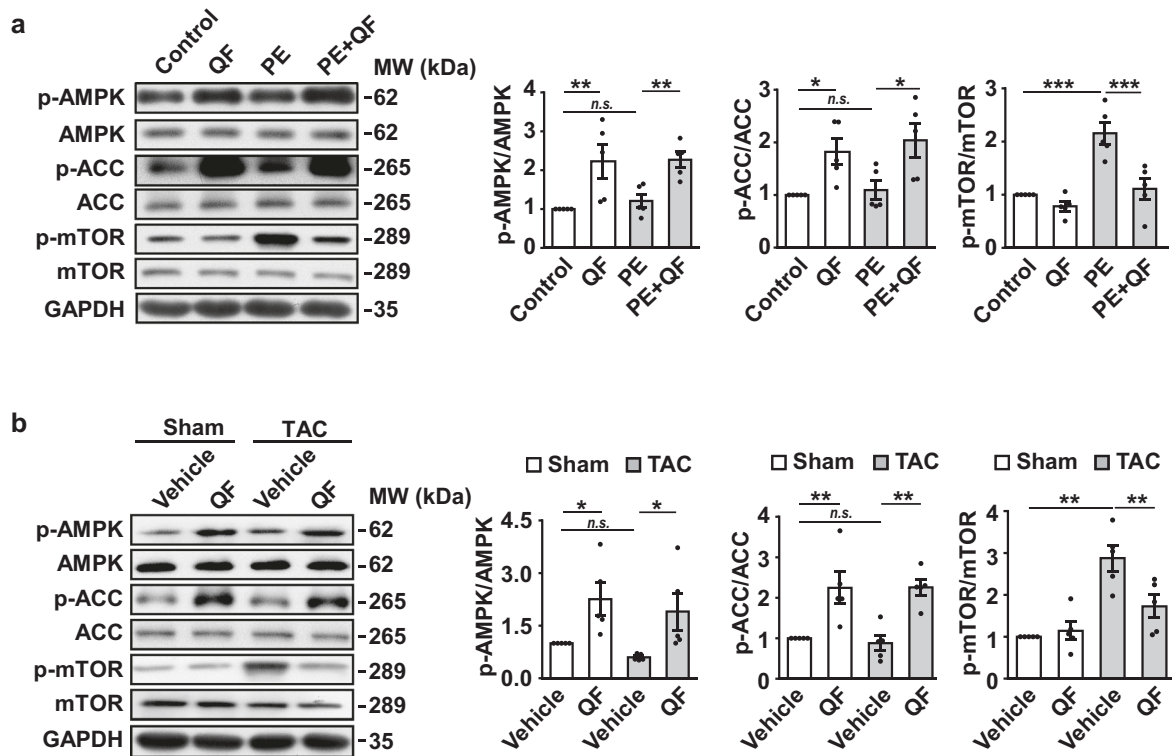


Fig. 4 QF84139 (QF) activates AMPK in NRCMs and the hearts from TAC mice. **a** Representative images (left panels) and averaged data (right panels) of immunoblot analysis for the total and phosphorylation level of AMPK, ACC, and mTOR in NRCMs exposed to PE with or without QF treatment. **b** Immunoblot analysis of total and phosphorylation level of AMPK, ACC, and mTOR in WT mice subjected to TAC or Sham surgery in the presence or absence of QF (15 mg·kg⁻¹·d⁻¹). GAPDH was used as loading control. *n* = 5 each. **P* < 0.05, ***P* < 0.01, ****P* < 0.001. n.s., nonsignificant

(Fig. 4a). It was further confirmed in the hearts from Sham and TAC mice (Fig. 4b). Acetyl-CoA carboxylase (ACC) is a direct downstream target of AMPK [27], we found that the QF84139 treatment elevated the phosphorylation level of ACC in the NRCMs with or without PE stimulation (Fig. 4a) and in the hearts from Sham and TAC mice (Fig. 4b). mTOR is a downstream target of AMPK [28]. We then examined the phosphorylation of mTOR and observed a significant decrease in the PE-enhanced phosphorylation level of mTOR after QF84139 treatment in the NRCMs, with the total protein level of mTOR was unchanged (Fig. 4a). The alterations were further confirmed in the hearts of Sham and TAC mice with QF84139 treatment (Fig. 4b). Moreover, the PE- and TAC-induced phosphorylation of 4E-BP1 and S6K was significantly inhibited after the QF84139 treatment (Supplementary Fig. S12), while the PE-induced phosphorylation of AKT was not affected by QF84139 (Supplementary Fig. S11). Therefore, QF84139 can activate AMPK signaling pathway in basal and hypertrophic conditions via an AKT-independent mechanism.

Inhibition of AMPK blocks effects of QF84139 against PE-induced cardiomyocyte hypertrophy

To verify the hypothesis that the protection of QF84139 against cardiac hypertrophy is mediated by the activation of AMPK, we treated NRCMs with a selective AMPK inhibitor Compound C (CpC) and an AMPK activator metformin. Indeed, compared with the control group, QF84139 increased the phosphorylation levels of AMPK and ACC as did by metformin, but this effect was blocked by CpC (Supplementary Fig. S13). Moreover, the role of AMPK in QF84139-mediated protection against hypertrophy was determined in the PE-induced cardiomyocyte hypertrophy model (Fig. 5a). As expected, the up-regulation of the mRNA of ANP, BNP and β-MHC stimulated by PE were significantly blocked in

metformin- and QF84139-treated groups, while these anti-hypertrophic effects were attenuated by CpC (Fig. 5b–d). Similar changes were observed in the protein level of ANP (Fig. 5e). The decreased cell size by QF84139 and metformin treatments under PE stimulation was also blocked by CpC (Fig. 5f, g). These results indicate that QF84139 attenuates PE-induced hypertrophic response in NRCMs via activating AMPK.

AMPKα2 knockdown cancels the protective effects of QF84139 against PE-induced cardiomyocyte hypertrophy

As mentioned above, AMPKα2 is the dominant form of AMPK in cardiomyocytes [11]. Thus, to further validate the contribution of AMPK, we knocked down AMPKα2 in NRCMs. The AMPKα2 mRNA level was significantly reduced by the AMPKα2 siRNA (Supplementary Fig. S14a), while the expression of AMPKα1 was not affected (Supplementary Fig. S14b). The downregulation of AMPKα2 completely blocked the anti-hypertrophic effect of QF84139 as indicated by the expression of cardiomyocyte hypertrophic marker genes (Fig. 6a–c), enlarged cell size (Fig. 6d, e), and ANP protein level (Fig. 6f) in the PE-stimulated NRCMs. These results suggest the key role of AMPKα2 in the anti-hypertrophic effect of QF84139.

AMPKα2 depletion abolishes the anti-hypertrophic effect of QF84139 in pressure overload-induced cardiac hypertrophy

The contribution of AMPKα2 to the cardioprotective role of QF84139 was further determined in mice with TAC. Vehicle or QF84139 (15 mg·kg⁻¹·d⁻¹) was intraperitoneally injected once daily for 2 weeks after Sham or TAC operation in the WT and AMPKα2 deficient (AMPKα2^{-/-}) littermates. There were no differences between WT and AMPKα2^{-/-} mice in basal condition (Supplementary Fig. S15). Western blot analysis demonstrated

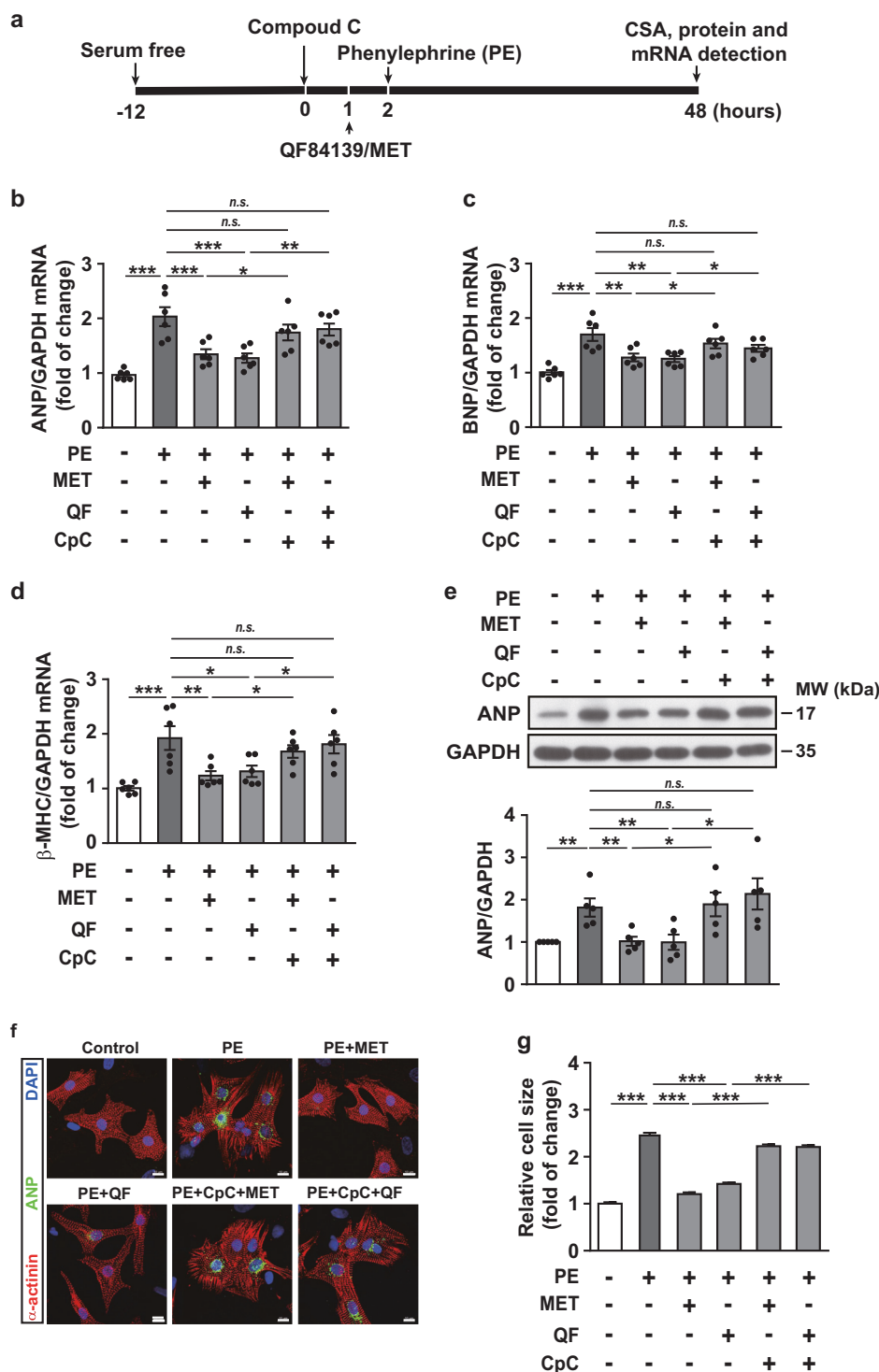


Fig. 5 Effects of QF84139 (QF) against PE-induced myocyte hypertrophy are blocked by compound C (CpC) in vitro. The NRCMs were treated with CpC for 1 h before addition with metformin (MET, 1 mM) or QF (3 μ M), and then stimulated with PE (10 μ M) for 48 h. **a** Schematic diagram of different treatments and analysis. qRT-PCR analysis of the mRNA expression of ANP (**b**), BNP (**c**) and β -MHC (**d**), $n = 6$. **e** Representative images (upper panels) and averaged data (lower panels) for immunoblot analysis of ANP in NRCMs. $n = 5$. Representative images (**f**) and averaged cell size (**g**) for immunofluorescence staining with anti- α -actinin antibody (red), anti-ANP antibody (green), and DAPI (blue) in NRCMs (200 random cells/heart, $n = 3$ hearts per group). Scale bar = 10 μ m. * $P < 0.05$, ** $P < 0.01$, *** $P < 0.001$. n.s., nonsignificant

the depletion of AMPK $\alpha 2$ in the hearts of AMPK $\alpha 2^{-/-}$ mice (Fig. 7a). Sustained treatment with QF84139 in the AMPK $\alpha 2^{-/-}$ littermates did not inhibit TAC-induced increases in the mRNA level of ANP and BNP (Fig. 7b) or the protein level of ANP (Fig. 7c). Moreover, in the AMPK $\alpha 2^{-/-}$ mice, the

echocardiographic analysis demonstrated that QF84139 failed to reverse TAC-induced cardiac dysfunction and remodeling (Fig. 7d), as indicated by the parameters such as EF (Fig. 7e), FS (Fig. 7f), LVPW;d (Fig. 7g), LVPW;s (Fig. 7h), IVS;d (Fig. 7i), IVS;s (Fig. 7j), and LV mass (Fig. 7k). In addition, the TAC-induced

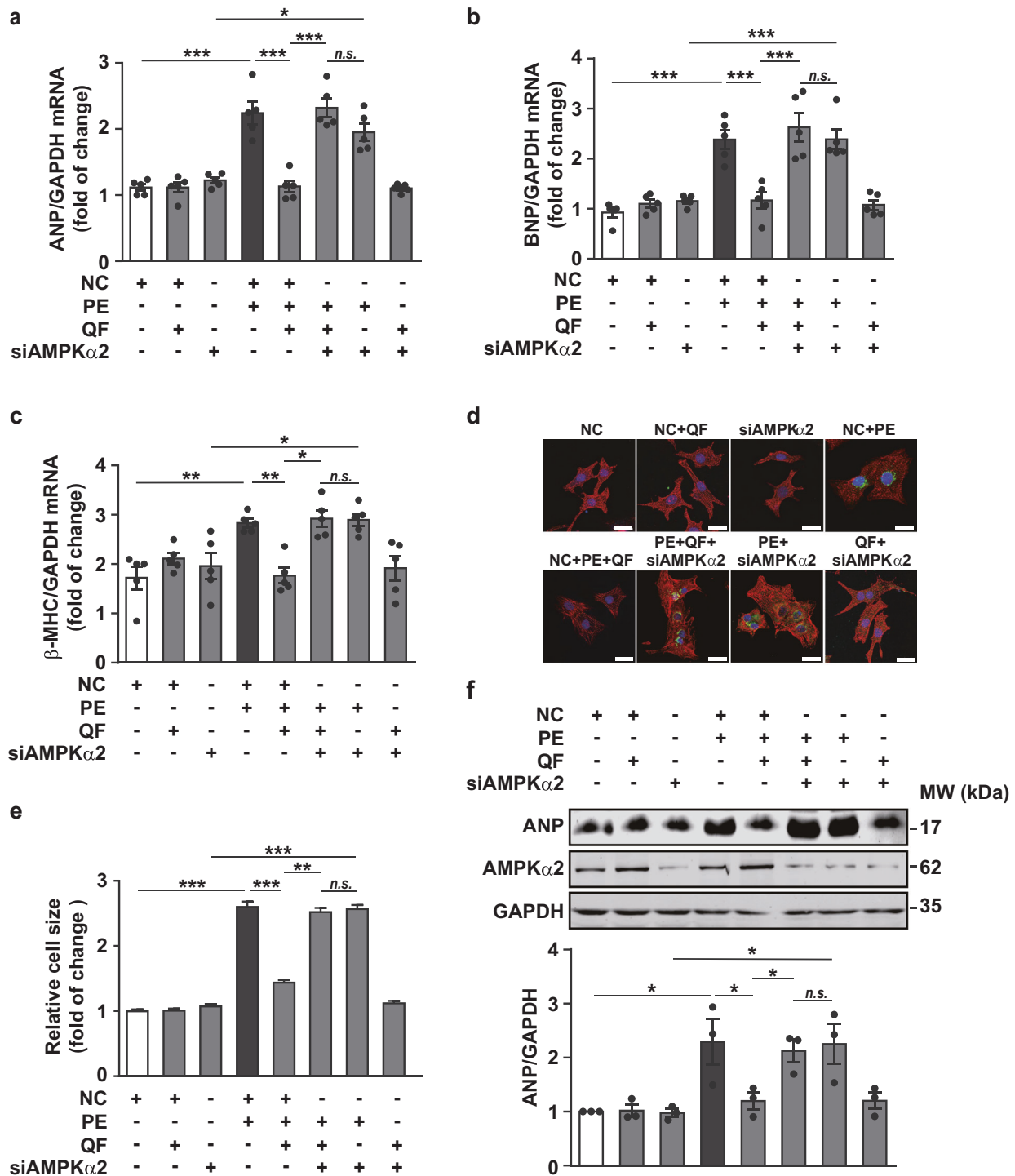


Fig. 6 QF84139 (QF) fails to inhibit PE-induced cardiac hypertrophy in AMPK α 2 knockdown NRCMs. **a–c** qRT-PCR analysis of mRNA expression levels of ANP, BNP, and β -MHC. $n=5$. Representative cardiomyocyte images (**d**) and averaged cell size (**e**) analyzed by immunofluorescence staining with anti- α -actinin antibody (red), anti-ANP antibody (green) and DAPI (blue) in NRCMs (200 random cells/heart, $n=3$ hearts per group). Scale bar = 20 μ m. **f** Representative images (upper panels) and averaged data (lower panels) for immunoblot analysis of ANP protein level in NRCMs. $n=3$. NC, negative control. * $P < 0.05$, ** $P < 0.01$, *** $P < 0.001$. n.s., nonsignificant

hypertrophic responses characterized by the enlarged heart sizes (Fig. 7l), increased ratios of HW/TL (Fig. 7m), HW/BW (Supplementary Fig. S16a), LW/TL (Supplementary Fig. S16b), LW/BW (Supplementary Fig. S16c), and augmented cross-sectional area (Fig. 7n) were still observed in the AMPK α 2^{-/-} mice even treated with QF84139. These data further confirmed AMPK activation is responsible for the anti-hypertrophic effect of QF84139.

DISCUSSION

In the present study, we demonstrated for the first time that (i) a synthesized natural product hybrid QF84139 inhibits the progression of PE-induced cardiomyocyte hypertrophy in vitro and the TAC-induced myocardial hypertrophy in vivo; (ii) QF84139 does not affect the activation of CaMKII δ , ERK, AKT, PKC ϵ , and P38 occurred in the hypertrophic cardiomyocytes, whereas it activates

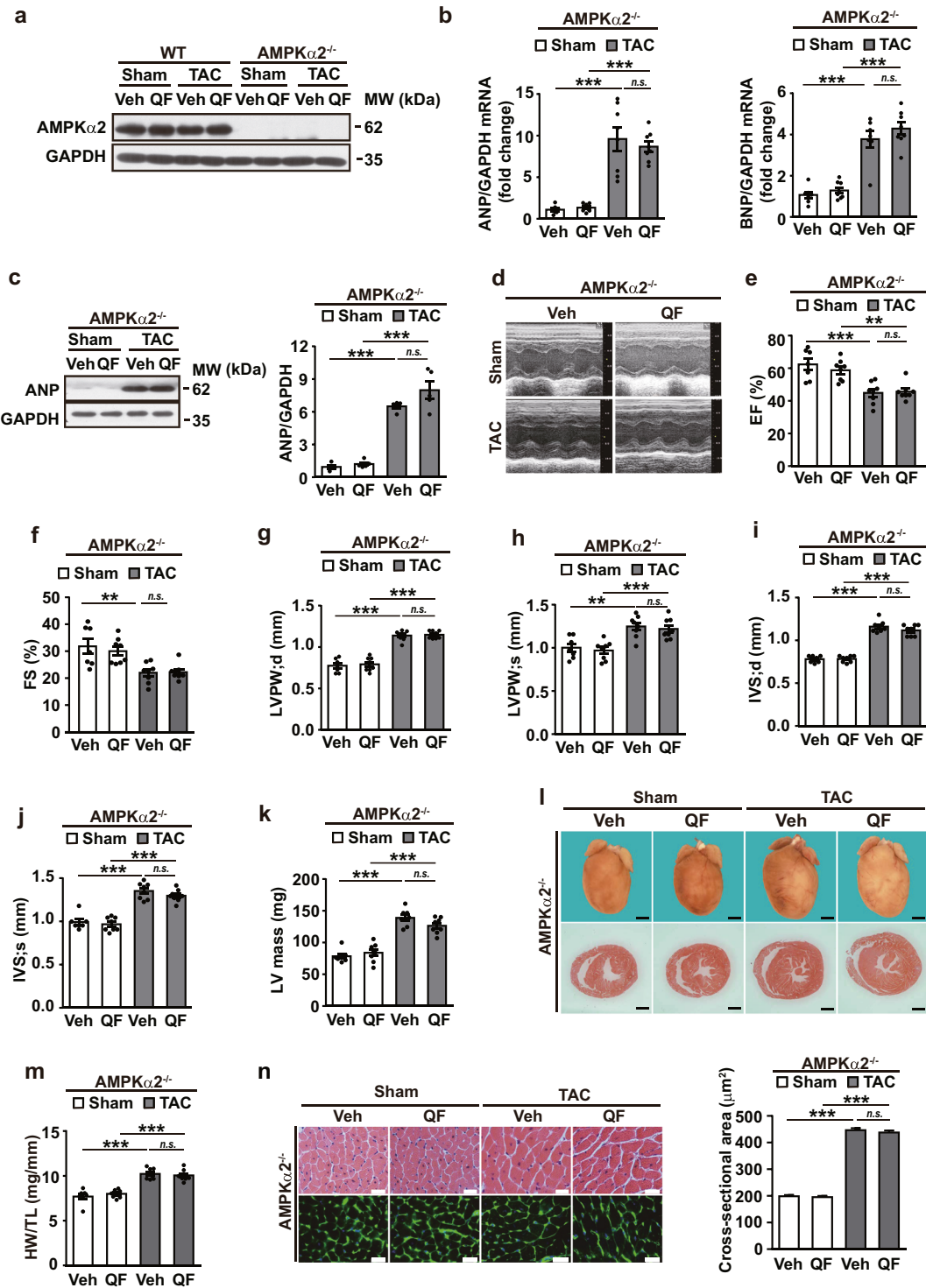


Fig. 7 QF84139 (QF) fails to inhibit pressure overload-induced cardiac hypertrophy in AMPK α 2^{-/-} mice. **a** Representative images of immunoblot analysis of AMPK α 2 in WT and AMPK α 2^{-/-} mice in the presence or absence of QF (15 mg·kg⁻¹·d⁻¹). **b** qRT-PCR analysis of mRNA expression levels of ANP and BNP. *n* = 8. **c** Representative images and averaged data of immunoblot analysis of ANP. *n* = 5. **d** Representative images of echocardiograms of AMPK α 2^{-/-} mice in the presence or absence of QF (15 mg·kg⁻¹·d⁻¹). **e** EF%, ejection fraction (%). **f** FS%, fractional shortening (%). **g** LVPW;d, left ventricle posterior wall thickness diastole. **h** LVPW;s, left ventricle posterior wall thickness systole. **i** IVS;d, interventricular septum diastolic dimension. **j** IVS;s, interventricular septum systolic dimension. **k** LV Mass, left ventricle mass. **l** Representative Gross morphology (top) and whole heart sections stained by H&E staining (bottom) of adult hearts from AMPK α 2^{-/-} mice. Scale bars = 1 mm. **m** Statistical results of heart weight/tibia length ratio (HW/TL). *n* = 8. **n** Left panels, representative H&E staining (top) and WGA staining (bottom) at 2 weeks post-TAC or Sham surgery. Scale bars = 20 μ m; right panel, quantification of cardiomyocyte size based on the cross-sectional area (200 random cells/heart, *n* = 3 hearts per group). ***P* < 0.01, ****P* < 0.001. n.s., nonsignificant

the AMPK signaling pathway in cardiomyocytes and hearts; and (iii) the anti-hypertrophic effect of QF84139 is canceled by AMPK inhibitor and knockdown of AMPK α 2 in the PE-treated cardiomyocytes and in the AMPK α 2^{-/-} mice. These data demonstrate that QF84139 attenuates cardiac hypertrophy via the activation of the AMPK signaling pathway and suggest that the activation of the AMPK signaling pathway can effectively reverse the cardiac hypertrophy even if the CaMKII δ , ERK, AKT, PKC ϵ , and P38 signaling pathways remain activated.

Cardiac hypertrophy is an important hallmark of pressure overload and a main cause of heart failure [1]. Thus, novel therapeutics for the cardiac hypertrophy is viewed as a most important goal for the treatment of heart diseases and is urgently needed [1, 29]. Ethnomedicine knowledge based drug discovery has been proven to be of great success in history [30, 31]. Traditional Chinese medicine (TCM) has been practiced for thousands of years and provided a vast source of pharmaceutical materials. Accumulating evidence indicate that traditional Chinese herbs are beneficial for cardiac hypertrophy exemplified by *Panax notoginse* [32, 33], *Ligusticum chuanxiong* [34], and *Scutellaria baicalensis* [35]. In this regard, natural products in these herbs responsible for cardiac hypertrophy might bring new hopes for the patients suffering from cardiac hypertrophy. The rhizomes of *Acorus tatarinowii* are commonly used to treat brain related disorders as well as heart diseases [36–38]. We have characterized pyrazine derivatives namely 2-(3',4'-dihydroxy-1'-butylenyl)-5-(2'',3'',4''-trihydroxybutyl)-pyrazine [39] and crotonine from *A. tatarinowii*. For the latter, it has also been isolated from the leaves of *Croton tiglium* with pronounced analgesic activity [40]. It is evident that these compounds possess a pyrazine core in the structure. Although several drugs such as glipizide, pyrazinamide, and zopiclone embrace this structure motif, we speculated that crotonine from *Acorus tatarinowii* might be a useful compound for the protection of heart. Indeed such structures like ligustrazine, a molecule from *Ligusticum chuanxiong*, have been proven to be beneficial for heart [41]. With this hypothesis, we have synthesized several crotonine-based scaffolds (data not shown) by using an oriented synthesis strategy inspired by the concept of powerful NPHs [42]. Among these, we found QF84139, a small molecule consisting of (–)-borneol, 5-(furan-2-yl)pyrazin-2(1*H*)-one which is a partial structure of natural product crotonine and a simple linker, shows potential protective roles in cardiac hypertrophy.

The TAC-induced cardiac hypertrophy model is broadly used to study anti-hypertrophic effect [2, 3]. In our study, the changes in LVPW;d, LVPW;s, LVS;d, LVS;s, LVID;d, and LV mass in TAC mice without QF84139 treatment are consistent with other reports [3, 43]. It is noticed that in our experiments the EF and FS are not significantly affected in WT mice after 2 weeks of TAC surgery (Supplementary Fig. S10b, c). The unchanged EF and FS are also observed by others [2, 3, 44, 45], though the decreased EF and FS are also reported [9]. The inconsistent observation might be caused by the degree of hypertrophy induced by the performance of the TAC operation. Supportively, the EF and FS were not altered in the first 2 weeks after TAC, but they significantly decreased at 5 and 8 weeks after TAC [2], demonstrating the negative correlation of the EF and FS with the severity of TAC model. In addition, we did observe the decreased EF and FS in AMPK α 2^{-/-} mice 2 weeks after TAC (Fig. 7e, f), suggesting the sensitivity of the mice hearts is subjected to hypertrophic stimuli after the deletion of AMPK α 2, an anti-hypertrophic factor [46, 47].

One important finding in this study is that QF84139 acts as a potent AMPK activator. We found that the AMPK signaling is significantly activated in both basic and hypertrophic conditions after QF84139 treatment (Fig. 4a, b), whereas the inhibition of AMPK activation by CpC (Fig. 5) or specific siRNA (Fig. 6) can block the anti-hypertrophic effect of QF84139 in the PE-stimulated cardiomyocytes. Moreover, the anti-hypertrophic effect of QF84139 is totally reversed in the AMPK α 2^{-/-} TAC mice (Fig. 7).

These data reveal that QF84139 exerts the anti-hypertrophic effect by activating the AMPK signaling pathway and suggest that QF84139 might act as a potent AMPK activator. The AMPK pathway is the primary mechanism in detecting and responding to changes in the cellular energy level [48]. It has been shown that AMPK activation can protect the heart from ischemic injury and pressure overload induced cardiac remodeling [49, 50], type 2 diabetes as well as other metabolic diseases and cancer [48]. The AMPK activation represents a potential target for the treatment of these diseases. Over the last few years, a significant development in the identifying of small molecule AMPK activators has been made, from which we understand the mechanism of these drugs to activate the kinases. Exploiting a new AMPK activator means opening up an exciting new therapeutic opportunity to the diseases that are related to AMPK signaling pathway. Up to now, AMPK activators can be classified as direct or indirect activators, based on the interaction of AMPK and the molecules [51]. The indirect activator activates AMPK by an increase of the AMP: ATP ratio [27], which is represented by metformin. Metformin is also a natural product-derivative originated from the plant *Galega officinalis* [52]. The activation of AMPK by metformin is based on the inhibition of complex I and thus leads to an increased AMP: ATP ratio [53]. The AMPK direct activator is binding directly to activate AMPK, which is represented by 5-aminoimidazole-4-carboxamide riboside (AICAR) that mimics the 5'-AMP and activates AMPK [51]. AICAR and metformin activate AMPK with different efficiency and mechanisms [54, 55]. They also have AMPK-independent functions. AICAR can inhibit P38 activation through AMPK independent pathway [56], while metformin can inhibit high-mobility group box 1-induced P38 activation and the activation of ERK without altering the phosphorylation level of AMPK [57]. In our results, QF84139 did not alter the phosphorylation level of p-P38, p-ERK or p-AKT (Supplementary Fig. S11), indicating that QF84139 can activate AMPK without affecting the activation of P38, ERK, and AKT. The different properties of these molecules may offer them to meet better application demands of patients with various conditions. Compared with the structure of AMPK activators based on patent literatures [51], QF84139 is different from them in the structure and represents a new type of structure scaffold of AMPK activators. Therefore, the finding of QF84139 may offer a new choice with clinical application potential. By further modification, QF84139-derivatives might be created with more power and safety. In addition, the QF84139 is a small molecule synthesized from tradition Chinese medicine, which would promote the modernization of Chinese traditional medicine.

Another novel finding here is that activation of the AMPK signaling pathway by QF84139 exerts powerful anti-hypertrophic effects in hearts and cardiomyocytes without affecting signaling pathways involved in the development of cardiac hypertrophy. Cardiac hypertrophy is usually associated with complex spectrum of pathophysiological alterations, such as cell death, fibrosis, Ca²⁺-handling protein dysregulation, mitochondrial dysfunction, metabolic reprogramming, etc. The signaling pathways of ERK, CaMKII δ , AKT, P38, and PKC ϵ mechanisms involved in these responses promote maladaptive cardiac hypertrophy and ultimately induce heart failure [1, 6, 8]. These signaling pathways are also activated in the PE-stimulated cardiomyocytes in the present study (Supplementary Fig. S11), whereas the phosphorylation level of AMPK remains unchanged in the cardiac hypertrophic models either induced by PE in the cardiomyocytes or by TAC in the mice. These observations are consistent with previous reports [3, 58]. Notably, QF84139 blocks the PE-induced cardiomyocyte hypertrophy without affecting these signaling pathways (Fig. 1b–g and Supplementary Fig. S11). These observations suggest that the kinases (ERK, CaMKII δ , AKT, P38, and PKC ϵ) might transduce signals to the same “molecular hub” that could be regulated by AMPK. mTOR might be a candidate for the regulation as the

phosphorylation of mTOR is significantly increased in the response to PE or TAC stimulation, while its activation is totally suppressed by the QF84139 treatment (Fig. 4a, b). mTOR is a well-known downstream target of AMPK and can be inhibited by the activation of AMPK through TSC complex [28]. The multiple faces of mTOR, including regulating protein synthesis, cell growth and proliferation, cell metabolism and stress responses [28], making it acts as a crucial protein in connecting the upstream stimuli and the downstream hypertrophic process [59, 60]. Supportively, mTOR could be inhibited by metformin [61] and no additive effects on AMPK activation are observed when use of QF84139 and metformin together (Supplementary Fig. S9), suggesting a similar effect of QF84139 with metformin on AMPK activation. Although mTOR-S2448 can be phosphorylated by AKT, in our results, the phosphorylation levels of AKT induced by PE and TAC were not affected by QF84139 (Supplementary Fig. S11). Taken together, the activation of the AMPK signaling pathway plays a crucial role in the attenuation of cardiac hypertrophy even if the signaling involved in the development of cardiac hypertrophy remain activated. The inhibition of mTOR might be responsible for the anti-cardiac hypertrophic effect of AMPK activation by QF84139. This possibility needs to be tested further. Moreover, how the QF84139-mediated AMPK activation results in the attenuation of mTOR phosphorylation at Ser2448 remains elusive and needs to be elucidated.

In conclusion, we reported a new type of natural product derivative QF84139 which attenuates cardiac hypertrophy induced by hypertrophic stimuli either in vitro or in vivo via the activation of AMPK. Moreover, we demonstrated that the activation of the AMPK signaling pathway by the QF84139 can significantly attenuate cardiac hypertrophy even if the hypertrophy-related signaling pathways are activated. Our findings also emphasize the value of natural product derivatives in the development of pharmacological therapy for cardiac hypertrophy and QF84139 would provide a promising lead compound for developing effective agents for the treatment of cardiac hypertrophy.

ACKNOWLEDGEMENTS

This work was supported by the National Natural Science Foundation of China (81770402; 81520108004 to H-tY), Strategic Priority Research Program of the CAS (No. XDA16010201 to HTY), National Key R&D Program of China (2017YFA0103700 to HTY), the research funding from Shanghai Jiao Tong University Affiliated Sixth People's Hospital to HTY and National Science Fund for Distinguished Young Scholars (81525026 to YXC). We thank Prof. Yong Ji (Nanjing Medical University, Nanjing, China) for valuable scientific advice. We also thank Dr. Jin-xi Wang and Dr. Shan-shan Gu (Shanghai Institute of Nutrition and Health, Shanghai, China) for the technical support.

AUTHOR CONTRIBUTIONS

Conception or design of the study: HTY, YXC, XXL, PZ, YY, YYZ; data collection: XXL, YY, PZ, YJZ, JJW, JLT, SYL, YMY; data analysis and interpretation: XXL, PZ, HTY, YXC, YYZ, YMY; drafting the manuscript: XXL, HTY, YXC, PZ, YY; financial support and final approval for the version to be published: HTY, YXC.

ADDITIONAL INFORMATION

Supplementary information The online version contains supplementary material available at <https://doi.org/10.1038/s41401-021-00678-5>.

Competing interests: The authors declare no competing interests.

REFERENCES

- Nakamura M, Sadoshima J. Mechanisms of physiological and pathological cardiac hypertrophy. *Nat Rev Cardiol.* 2018;15:387–407.
- Ren Z, Yu P, Li D, Li Z, Liao Y, Wang Y, et al. Single-cell reconstruction of progression trajectory reveals intervention principles in pathological cardiac hypertrophy. *Circulation.* 2020;141:1704–19.
- Ritterhoff J, Young S, Villet O, Shao D, Neto FC, Bettcher LF, et al. Metabolic remodeling promotes cardiac hypertrophy by directing glucose to aspartate biosynthesis. *Circ Res.* 2020;126:182–96.
- Gogiraju R, Bochenek ML, Schafer K. Angiogenic endothelial cell signaling in cardiac hypertrophy and heart failure. *Front Cardiovasc Med.* 2019;6:20.
- Tran DH, Wang ZV. Glucose metabolism in cardiac hypertrophy and heart failure. *J Am Heart Assoc.* 2019;8:e012673.
- Gao W, Guo N, Zhao S, Chen Z, Zhang W, Yan F, et al. HTR2A promotes the development of cardiac hypertrophy by activating PI3K-PDK1-AKT-mTOR signaling. *Cell Stress Chaperones.* 2020;25:899–908.
- Shimizu I, Minamoto T. Physiological and pathological cardiac hypertrophy. *J Mol Cell Cardiol.* 2016;97:245–62.
- Li Y, Feng L, Li G, An J, Zhang S, Li J, et al. Resveratrol prevents ISO-induced myocardial remodeling associated with regulating polarization of macrophages through VEGF-B/AMPK/NF- κ B pathway. *Int Immunopharmacol.* 2020;84:106508.
- Li H, Xu JD, Fang XH, Zhu JN, Yang J, Pan R, et al. Circular RNA circRNA_000203 aggravates cardiac hypertrophy via suppressing miR-26b-5p and miR-140-3p binding to Gata4. *Cardiovasc Res.* 2020;116:1323–34.
- Feng Y, Zhang Y, Xiao H. AMPK and cardiac remodelling. *Sci China Life Sci.* 2018; 61:14–23.
- Zhang P, Hu X, Xu X, Fassett J, Zhu G, Viollet B, et al. AMP activated protein kinase- α 2 deficiency exacerbates pressure-overload-induced left ventricular hypertrophy and dysfunction in mice. *Hypertension.* 2008;52:918–24.
- Lin H, Li Y, Zhu H, Wang Q, Chen Z, Chen L, et al. Lansoprazole alleviates pressure overload-induced cardiac hypertrophy and heart failure in mice by blocking the activation of beta-catenin. *Cardiovasc Res.* 2020;116:101–13.
- Meshima S, Okada M, Yamawaki H. Eukaryotic elongation factor 2 (eEF2) kinase/eEF2 plays protective roles against glucose deprivation-induced cell death in H9c2 cardiomyoblasts. *Apoptosis.* 2019;24:359–68.
- Xu X, Lu Z, Fassett J, Zhang P, Hu X, Liu X, et al. Metformin protects against systolic overload-induced heart failure independent of AMP-activated protein kinase α 2. *Hypertension.* 2014;63:723–8.
- Li L, Zhang Q, Zhang X, Zhang J, Wang X, Ren J, et al. Microtubule associated protein 4 phosphorylation leads to pathological cardiac remodeling in mice. *EBioMedicine.* 2018;37:221–35.
- Qi H, Ren J, Ba L, Song C, Zhang Q, Cao Y, et al. MSTN attenuates cardiac hypertrophy through inhibition of excessive cardiac autophagy by blocking AMPK/mTOR and miR-128/PPARG/NF- κ B. *Mol Ther Nucleic Acids.* 2020;19:507–22.
- Zuo A, Zhao X, Li T, Li J, Lei S, Chen J, et al. CTRP9 knockout exaggerates lipotoxicity in cardiac myocytes and high-fat diet-induced cardiac hypertrophy through inhibiting the LKB1/AMPK pathway. *J Cell Mol Med.* 2020;24:2635–47.
- Dziubak A, Wojcicka G, Wojtak A, Beltowski J. Metabolic effects of metformin in the failing heart. *Int J Mol Sci.* 2018;19:2869.
- Grahame Hardie D. Regulation of AMP-activated protein kinase by natural and synthetic activators. *Acta Pharm Sin B.* 2016;6:1–19.
- Newman DJ, Cragg GM. Natural products as sources of new drugs over the nearly four decades from 01/1981 to 09/2019. *J Nat Prod.* 2020;83:770–803.
- Tietze LF, Bell HP, Chandrasekhar S. Natural product hybrids as new leads for drug discovery. *Angew Chem Int Ed Engl.* 2003;42:3996–4028.
- Baranyai Z, Kratky M, Vinsova J, Szabo N, Senoner Z, Horvati K, et al. Combating highly resistant emerging pathogen mycobacterium abscessus and mycobacterium tuberculosis with novel salicylanilide esters and carbamates. *Eur J Med Chem.* 2015;101:692–704.
- Wang Z, Zhang XJ, Ji YX, Zhang P, Deng KQ, Gong J, et al. The long noncoding RNA Chaer defines an epigenetic checkpoint in cardiac hypertrophy. *Nat Med.* 2016;22:1131–9.
- Gu S, Tan J, Li Q, Liu S, Ma J, Zheng Y, et al. Downregulation of LAPTM4B contributes to the impairment of the autophagic flux via unopposed activation of mTORC1 signaling during myocardial ischemia/reperfusion injury. *Circ Res.* 2020;127:e148–e165.
- Lu X, He Y, Tang C, Wang X, Que L, Zhu G, et al. Triad3A attenuates pathological cardiac hypertrophy involving the augmentation of ubiquitination-mediated degradation of TLR4 and TLR9. *Basic Res Cardiol.* 2020;115:19.
- Wang J, Liu M, Wu Q, Li Q, Gao L, Jiang Y, et al. Human embryonic stem cell-derived cardiovascular progenitors repair infarcted hearts through modulation of macrophages via activation of signal transducer and activator of transcription 6. *Antioxid Redox Signal.* 2019;31:369–86.
- Salt IP, Hardie DG. AMP-activated protein kinase: an ubiquitous signaling pathway with key roles in the cardiovascular system. *Circ Res.* 2017;120:1825–41.
- Laplante M, Sabatini DM. mTOR signaling at a glance. *J Cell Sci.* 2009;122: 3589–94.
- Reid BG, Stratton MS, Bowers S, Cavasin MA, Demos-Davies KM, Susano I, et al. Discovery of novel small molecule inhibitors of cardiac hypertrophy using high throughput, high content imaging. *J Mol Cell Cardiol.* 2016;97:106–13.

30. Fabricant DS, Farnsworth NR. The value of plants used in traditional medicine for drug discovery. *Environ Health Perspect.* 2001;109:69–75.
31. Gurib-Fakim A. Medicinal plants: traditions of yesterday and drugs of tomorrow. *Mol Asp Med.* 2006;27:1–93.
32. Xiao J, Zhu T, Yin YZ, Sun B. Notoginsenoside R1, a unique constituent of *Panax notoginseng*, blinds proinflammatory monocytes to protect against cardiac hypertrophy in ApoE^{-/-} mice. *Eur J Pharmacol.* 2018;833:441–50.
33. Zhang B, Zhang J, Zhang C, Zhang X, Ye J, Kuang S, et al. Notoginsenoside R1 protects against diabetic cardiomyopathy through activating estrogen receptor alpha and its downstream signaling. *Front Pharmacol.* 2018;9:1227.
34. Luo M, Chen PP, Yang L, Wang P, Lu YL, Shi FG, et al. Sodium ferulate inhibits myocardial hypertrophy induced by abdominal coarctation in rats: involvement of cardiac PKC and MAPK signaling pathways. *Biomed Pharmacother.* 2019;112:108735.
35. Chen HM, Hsu JH, Liou SF, Chen TJ, Chen LY, Chiu CC, et al. Baicalein, an active component of *Scutellaria baicalensis* Georgi, prevents lysophosphatidylcholine-induced cardiac injury by reducing reactive oxygen species production, calcium overload and apoptosis via MAPK pathways. *BMC Complement Alter Med.* 2014;14:233.
36. Mao J, Huang S, Liu S, Feng XL, Yu M, Liu J, et al. A herbal medicine for Alzheimer's disease and its active constituents promote neural progenitor proliferation. *Aging Cell.* 2015;14:784–96.
37. Lee HJ, Ahn SM, Pak ME, Jung DH, Lee SY, Shin HK, et al. Positive effects of alpha-sarone on transplanted neural progenitor cells in a murine model of ischemic stroke. *Phytomedicine.* 2018;51:151–61.
38. Hui S, Yang Y, Peng WJ, Sheng CX, Gong W, Chen S, et al. Protective effects of Bushen Tiansui decoction on hippocampal synapses in a rat model of Alzheimer's disease. *Neural Regen Res.* 2017;12:1680–6.
39. Tong XG, Qiu B, Luo GF, Zhang XF, Cheng YX. Alkaloids and sesquiterpenoids from *Acorus tatarinowii*. *J Asian Nat Prod Res.* 2010;12:438–42.
40. Wu XA, Zhao YM, Yu NJ. A novel analgesic pyrazine derivative from the leaves of *Croton tiglium* L. *J Asian Nat Prod Res.* 2007;9:437–41.
41. Liu W, Zi M, Naumann R, Ulm S, Jin J, Taglieri DM, et al. Pak1 as a novel therapeutic target for antihypertrophic treatment in the heart. *Circulation.* 2011;124:2702–15.
42. Mehta G, Singh V. Hybrid systems through natural product leads: an approach towards new molecular entities. *Chem Soc Rev.* 2002;31:324–34.
43. Lee A, Jeong D, Mitsuyama S, Oh JG, Liang L, Ikeda Y, et al. The role of SUMO-1 in cardiac oxidative stress and hypertrophy. *Antioxid Redox Signal.* 2014;21:1986–2001.
44. Shende P, Xu L, Morandi C, Pentassuglia L, Heim P, Lebboukh S, et al. Cardiac mTOR complex 2 preserves ventricular function in pressure-overload hypertrophy. *Cardiovasc Res.* 2016;109:103–14.
45. Matsuo K, Shibata R, Ohashi K, Kambara T, Uemura Y, Hiramatsu-Ito M, et al. Omentin functions to attenuate cardiac hypertrophic response. *J Mol Cell Cardiol.* 2015;79:195–202.
46. Li Y, Chen C, Yao F, Su Q, Liu D, Xue R, et al. AMPK inhibits cardiac hypertrophy by promoting autophagy via mTORC1. *Arch Biochem Biophys.* 2014;558:79–86.
47. Stuck BJ, Lenski M, Bohm M, Laufs U. Metabolic switch and hypertrophy of cardiomyocytes following treatment with angiotensin II are prevented by AMP-activated protein kinase. *J Biol Chem.* 2008;283:32562–9.
48. Myers RW, Guan HP, Ehrhart J, Petrov A, Prahalada S, Tozzo E, et al. Systemic pan-AMPK activator MK-8722 improves glucose homeostasis but induces cardiac hypertrophy. *Science.* 2017;357:507–11.
49. Chen Y, Ge Z, Huang S, Zhou L, Zhai C, Chen Y, et al. Delphinidin attenuates pathological cardiac hypertrophy via the AMPK/NOX/MAPK signaling pathway. *Aging.* 2020;12:5362–83.
50. Deng W, Zong J, Bian Z, Zhou H, Yuan Y, Zhang R, et al. Indole-3-carbinol protects against pressure overload induced cardiac remodeling via activating AMPK-alpha. *Mol Nutr Food Res.* 2013;57:1680–7.
51. Kim J, Yang G, Kim Y, Kim J, Ha J. AMPK activators: mechanisms of action and physiological activities. *Exp Mol Med.* 2016;48:e224.
52. Apostolova N, Iannantuoni F, Gruevska A, Muntane J, Rocha M, Victor VM. Mechanisms of action of metformin in type 2 diabetes: effects on mitochondria and leukocyte-endothelium interactions. *Redox Biol.* 2020;34:101517.
53. Hawley SA, Ross FA, Chevztzoff C, Green KA, Evans A, Fogarty S, et al. Use of cells expressing gamma subunit variants to identify diverse mechanisms of AMPK activation. *Cell Metab.* 2010;11:554–65.
54. Li Y, Su J, Sun W, Cai L, Deng Z. AMP-activated protein kinase stimulates osteoblast differentiation and mineralization through autophagy induction. *Int J Mol Med.* 2018;41:2535–44.
55. Chen D, Wang Y, Wu K, Wang X. Dual effects of metformin on adipogenic differentiation of 3T3-L1 preadipocyte in AMPK-dependent and independent manners. *Int J Mol Sci.* 2018;19:1547.
56. Quan H, Kim JM, Lee HJ, Lee SH, Choi JI, Bae HB. AICAR enhances the phagocytic ability of macrophages towards apoptotic cells through P38 mitogen activated protein kinase activation independent of AMP-activated protein kinase. *PLoS One.* 2015;10:e0127885.
57. Gou S, Cui P, Li X, Shi P, Liu T, Wang C. Low concentrations of metformin selectively inhibit CD133⁺ cell proliferation in pancreatic cancer and have anticancer action. *PLoS One.* 2013;8:e63969.
58. Fu YN, Xiao H, Ma XW, Jiang SY, Xu M, Zhang YY. Metformin attenuates pressure overload-induced cardiac hypertrophy via AMPK activation. *Acta Pharmacol Sin.* 2011;32:879–87.
59. Sciarretta S, Forte M, Frati G, Sadoshima J. New insights into the role of mTOR signaling in the cardiovascular system. *Circ Res.* 2018;122:489–505.
60. Sciarretta S, Volpe M, Sadoshima J. Mammalian target of rapamycin signaling in cardiac physiology and disease. *Circ Res.* 2014;114:549–64.
61. Dowling RJ, Zakikhani M, Fantus IG, Pollak M, Sonenberg N. Metformin inhibits mammalian target of rapamycin-dependent translation initiation in breast cancer cells. *Cancer Res.* 2007;67:10804–12.